Electrical magnetotransport properties in $R\mathrm{Co}_{12}\mathrm{B}_6$ compounds ($R = $ Y, Gd, and Ho)

F. Mesquita,[*] S. G. Magalhaes, and P. Pureur[†]

Instituto de Física, Universidade Federal do Rio Grande do Sul, 91501-970 Porto Alegre, Rio Grande do Sul, Brazil

L. V. B. Diop[‡]

Université de Lorraine, CNRS, IJL, F-54000 Nancy, France

O. Isnard

Université Grenoble Alpes, Institut Néel, CNRS BP166x, 38042 Grenoble Cedex, France

Remarkable electronic transport and magnetotransport properties are found in the intermetallic compounds $R\mathrm{Co}_{12}\mathrm{B}_6$ ($R = $ Y, Ho, and Gd). Detailed resistivity, magnetoresistance, and Hall effect measurements are reported in the temperature range between 2 and 320 K under applied magnetic fields up to 9 T. Auxiliary magnetization results and structural data are also reported. The magnetic ordering observed in these systems depends on the rare-earth atom. In the $\mathrm{YCo}_{12}\mathrm{B}_6$ compound, a ferromagnetic-type ordering is observed ($T_C \approx$ 149 K) whereas the $\mathrm{GdCo}_{12}\mathrm{B}_6$ and $\mathrm{HoCo}_{12}\mathrm{B}_6$ compounds show ferrimagnetic-type ordering ($T_C \approx 162$ and 144 K, respectively) and their magnetization exhibits the compensation phenomenon. All compounds show high residual-resistance ratio (RRR) rates and resistivities typical of magnetically ordered systems, with a characteristic downward inflection at the critical temperature. The resistivity results are described in terms of the interplay between the electron-phonon interaction and a magnetic term. The magnetoresistance is consequence of a complex superposition of effects due to conduction in spin-polarized bands and to spin-disorder suppression. A strong positive contribution, which prevails at low temperatures, is described with a basis on the Campbell-Fert model that assumes conduction by two spin-polarized currents with a spin-mixing term. The usual negative effect related to suppression of spin disorder becomes the dominant contribution at intermediate- and high-temperature regimes. At low temperatures, the Hall resistivity results are also consistent with conduction by two spin-polarized bands. Moreover, a sign reversal observed in the Hall resistivity for all compounds at low temperatures indicates that the majority spin-up band is holelike, while the minority spin band is electronlike. The ordinary and anomalous Hall contributions could be separated. The intrinsic Karplus-Luttinger mechanism is the most relevant contribution to the anomalous Hall resistivity in all studied compounds. However, an additional term due to chiralities related to canting of the Co moments also plays a role in the temperature region near T_C.

I. INTRODUCTION

Some intermetallic ferrimagnetic compounds usually based on rare-earth and transition-metal elements present the very interesting phenomenon known as the compensation temperature point, T_{comp}. At this particular temperature, the oppositely oriented magnetization of the two sublattices have approximately the same magnitude, so that the global magnetization goes through a deep and sharp minimum. As a consequence of their unusual magnetic properties, these systems have been considered as potentially attractive for applications in spintronics or magneto-optical recording [1].

In particular, a renewed interest has arisen recently in the study of such ferrimagnetic materials in the context of ultra-fast magnetization reversal of magnetic memories and optical switching devices [2,3]. In spite of these facts, the electrical properties of these materials have received little attention until now [4–6].

Among the ferrimagnetic compounds presenting the compensation property, the $RTM_{12}\mathrm{B}_6$ family, where R is a rare-earth atom and TM is a transition-metal element, occupies a special place. This series of compounds crystallizes in the rhombohedral $\mathrm{SrNi}_{12}\mathrm{B}_6$-type structure (space group $R\bar{3}m$) [7,8]. In such a crystal arrangement, the rare-earth element (R) and boron (B) have unique crystallographic positions. However, the transition-metal atoms (TM) are located in two inequivalent crystallographic sites. These compounds exhibit magnetic order below room temperature, with Curie temperature ranging around 150 K. Several noticeable developments have recently been reported concerning this family of materials. A remarkable example is the discovery of

---

[*]fabiano.mesquita@ufrgs.br; Also at Université Grenoble Alpes, Institut Néel, CNRS BP166x, 38042 Grenoble Cedex, France.

[†]ppureur@ufrgs.br

[‡]Also at Université Grenoble Alpes, Institut Néel, CNRS BP166x, 38042 Grenoble Cedex, France.

the nonconventional and discontinuous magnetization process featured by dramatically sharp steps, as in $LaFe_{12}B_6$ [9–12].

The $RCo_{12}B_6$ compounds have been found to be stable along the whole lanthanide series. These systems have attracted much interest because of their complex magnetic phase diagrams, the existence of a compensation point, and a remarkably small Co magnetic moment [8,13,14]. Their magnetic behavior is dominated by the interactions R-Co and Co-Co [15], the R-R interactions being usually much weaker or negligible. The magnetic ordering temperature is weakly dependent on the rare-earth element. For example, the compound $YCo_{12}B_6$ orders below 150 K [14] while the systems containing Gd and Ho order at 162 and 145 K, respectively. Both $GdCo_{12}B_6$ and $HoCo_{12}B_6$ are ferrimagnets, the magnetization of the R sublattice being dominant at low temperatures, and that related to the Co atoms being larger above T_{comp} where magnetization for both magnetic sublattices cancels out. The experimental values of the compensation temperature are $T_{comp} = 49$ and 44 K for $GdCo_{12}B_6$ [16] and $HoCo_{12}B_6$ [17], respectively. In spite of the difficulties in performing neutron diffraction on heavy neutron absorbers like the boride compounds, the magnetic structure of some of these $RCo_{12}B_6$ compounds has recently been reported for $R =$ La [18], Gd [13], and Ho [17]. These experiments reveal the occurrence of spin canting in the Co sublattice. Mössbauer spectroscopy [13] and nuclear magnetic resonance (NMR) [19,20] results confirm this neutron diffraction finding. In particular, at $T = 2$ K, $LaCo_{12}B_6$ exhibits a conical structure with Co magnetic moments tilted 60° away from the hexagonal c axis [18]. The $GdCo_{12}B_6$ compound has an almost axial magnetic structure. The global moment has a small tilt angle of 17° away from the c axis at 4 K [13]. The magnetic structure of the $HoCo_{12}B_6$ has attracted more interest since it exhibits a spin reorientation phenomenon at $T_{SR} = 76$ K [17,21]. The global magnetic moment is aligned nearly parallel to the c axis at the lowest temperatures and becomes reorient toward the basal (a, b) plane above T_{SR}. This spin reorientation transition has been described as resulting from the competition between the magnetocrystalline anisotropies due to the Ho and Co sublattice, respectively [17]. Though the structural and magnetic properties of the intermetallic compounds $RT_{12}B_6$ have been extensively studied over the past 50 years [7–16], only a few works address the electrical resistivity on these systems [4–6]. To our knowledge, no investigations have been reported on magnetotransport properties such as magnetoresistance and the Hall effect, although a study on low-frequency magnetoimpedance was recently published [6].

In this paper, we carry out an extensive experimental study of the electrical resistivity, magnetoresistance, and Hall effect of $RCo_{12}B_6$ model compounds. We focus our attention on those where $R =$ Y, Gd, and Ho. The choice of Y enables us to probe the Co magnetic sublattice alone, whereas the selection of Gd and Ho offers the opportunity to investigate the additional effects of the rare-earth magnetic sublattice. Since the Gd- and Ho-based compounds are also used as model systems exhibiting the compensation point phenomenon, our results allow us to correlate this characteristic with the transport properties. From the magnetoresistance experiments, at very low applied field the spontaneous anisotropy of the resistivity

was estimated for the compounds where $R =$ Y and Gd. These results lead to further information on the spin-polarized currents in these compounds. Hall effect measurements are presented and analyzed, so that the ordinary and anomalous contributions could be separated. To probe the conduction by the two spin-polarized currents and determine the majority carriers, we have investigated all of the Hall coefficients for all compounds and their temperature dependences. Analysis of the anomalous Hall effect measurements will be used to get the different contributions and discuss their origin in light of the knowledge of the magnetic structures.

II. EXPERIMENT

Polycrystalline samples of $RCo_{12}B_6$, with $R =$ Y, Gd, and Ho, were prepared by melting the appropriate amounts of the high-purity elements ($>99, 95\%$) in an induction furnace under a purified argon atmosphere. The resulting polycrystalline ingots were annealed at 900 °C over the course of three weeks. Detailed information about the synthesis process can be found in Ref. [16]. The prepared samples were analyzed by x-ray diffraction (XRD) and energy-dispersive x-ray spectroscopy (EDS). Samples for transport measurements were cut out from the obtained ingots by spark-cutting into an appropriate geometry. The resistivity, magnetoresistance, and Hall effect measurements were performed with the ACTS modulus of a Quantum Design PPMS system. The resistivity and magnetoresistance data were obtained by using the usual four-point contact configuration. Measurements were carried out according to the following configurations: (i) magnetic field applied perpendicular to the current ($H \perp i$) and (ii) field applied parallel to the current orientation ($H \parallel i$). For the Hall effect experiments, two additional lateral contacts were placed on the samples. A microtype welding apparatus was used for fixing the electrical contact on the samples' surface. Isothermal magnetization measurements in fields up to 10 T were carried out at several temperatures in the range 4–300 K. These experiments were performed using the extraction method of a home-made magnetometer, which is described in Ref. [22]. These last measurements were mostly used as complementary in Hall effect analysis. All magnetotransport experiments were done in temperatures ranging between 2 and 325 K, upon applied magnetic fields varying between the limits ±9 T.

III. RESULTS AND DISCUSSION

A. Structural and magnetic properties

The analysis of the x-ray diffraction diagrams confirms that the $R\overline{3}m$ space group symmetry is retained for the studied intermetallic compounds. The derived unit-cell parameters at room temperature are summarized in Table I. The obtained values are in good agreement with previous reports [7,8]. The temperature dependence of magnetization, measured upon heating of the zero-field-cooled materials in an applied magnetic field of 0.1 T, is displayed in Fig. 1. The thermomagnetic curves indicate that the ground state is ferromagnetic for $YCo_{12}B_6$ and ferrimagnetic with a compensation point for Gd- and Ho-based compounds. Moreover, $HoCo_{12}B_6$ shows an anomaly at about 76 K corresponding to a spontaneous

TABLE I. Lattice parameters obtained from x-ray diffraction (XRD) experiments on $R\text{Co}_{12}\text{B}_6$ (R = Y, Gd, and Ho).

Parameters	$R\text{Co}_{12}\text{B}_6$		
	Y	Gd	Ho
a (Å)	9.445 ± 8	9.455 ± 4	9.451 ± 2
c (Å)	7.438 ± 2	7.449 ± 1	7.454 ± 3
V (Å^3)	574.6 ± 5	576.7 ± 4	576.6 ± 4

spin reorientation transition in which a rotation of the magnetization vector with respect to the crystallographic axes takes place upon a change in temperature. In Fig. 2 we compare the magnetization isotherms recorded at 4 K of the thermally demagnetized $R\text{Co}_{12}\text{B}_6$ alloys. The magnetization of $Y\text{Co}_{12}\text{B}_6$ saturates at low magnetic field following steep initial growth. A large susceptibility can be seen at the high-field portions of the magnetization isotherms for $Ho\text{Co}_{12}\text{B}_6$ and, to a lesser extent, for $Gd\text{Co}_{12}\text{B}_6$ systems. This large slope is characteristic of the progressive alignment of the magnetic moments of the Co and Gd/Ho sublattices along the external applied magnetic field [16,17]. More details on the structural and magnetic properties of these $R\text{Co}_{12}\text{B}_6$ compounds, including neutron diffraction investigations or high magnetic field studies, can be found in Refs. [8,13,14,16,17].

B. Resistivity

Resistivity measurements as a function of temperature are shown in Fig. 3 for all studied compounds. The observed $\rho(T)$ curves are typical of magnetically ordered systems, in which the transition from the paramagnetic phase to the ordered state is signaled by a characteristic steeplike decrease around the critical temperature. We interpret the results in Fig. 3 by assuming that three predominant electronic scattering mechanisms describe the temperature dependence of the resistivity in the studied compounds. At very low temperatures a residual term, ρ_0, due to static disorder is dominant. Also relevant
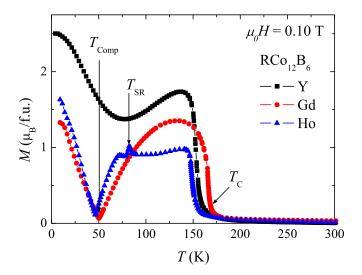

FIG. 2. Magnetization as a function of applied magnetic field for $Y\text{Co}_{12}\text{B}_6$, $Gd\text{Co}_{12}\text{B}_6$, and $Ho\text{Co}_{12}\text{B}_6$ at $T = 4$ K.

is the interaction between the lattice collective excitations (phonons) and the conduction electrons. A third important contribution is due to the electron scattering by the thermal disorder of the spin system. An analysis of the relative weight and the temperature dependence of these resistivity contributions is shown in Fig. 3 for the three studied compounds. The magnitude of ρ_0 is rather small, considering that the three investigated systems are structurally complex intermetallics. This fact is expressed by the high residual resistivity ratios (RRR) listed in Table II. To estimate the contribution due to the electron-phonon interaction, $\rho_{\text{ph}}(T)$, we adopt the single-band Bloch-Grüneisen approach [23], according to which

$$\rho_{\text{ph}}(T) = 4\rho_\theta \left(\frac{T}{\theta_R}\right)^5 J_5\left(\frac{\theta_R}{T}\right), \tag{1}$$

where ρ_θ is proportional to the strength of the electron-phonon coupling, θ_R is the Debye temperature as estimated from resistivity measurements, and J_5 is a Debye integral [23]. By combining the limits of Eq. (1) at high temperatures ($\rho_{\text{ph}} \propto T$) and at low temperatures ($\rho_{\text{ph}} \propto T^5$) and assuming that the slope $d\rho/dT$ of the measured resistivity well above T_C [see the red dashed lines in panels (a)–(c) of Fig. 3] is solely due to ρ_{ph}, we determined the parameters ρ_θ and θ_R. Then, Eq. (1) was employed to calculate the contribution $\rho_{\text{ph}}(T)$ in the whole temperature range. These results are shown as the red pointlike line in Fig. 3. The estimated parameters ρ_θ and θ_R are listed in Table II for all studied compounds. Both parameters vary systematically along the series of compounds, suggesting that their values are related to the difference between the atomic masses of Y and lanthanide atoms Gd and Ho, indicating that the phonon spectra of the studied $R\text{Co}_{12}\text{B}_6$ systems are basically similar, although renormalized by the rare-earth mass.

The resistivity data in Fig. 3 for all the studied compounds deviate from the linear temperature dependence when approaching the ordering temperature upon cooling. This effect is a consequence of the progressive establishment of the cooperative magnetic ordering. Below the magnetic
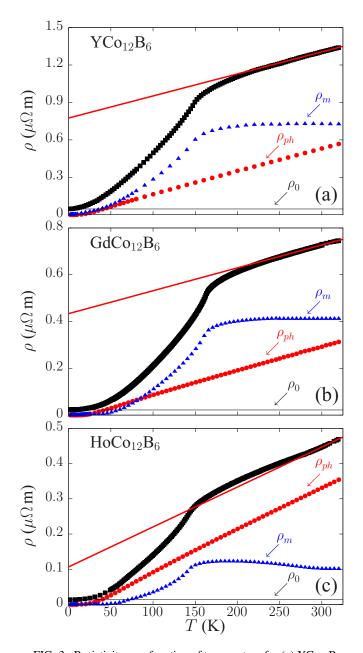

FIG. 1. Magnetization as a function of temperature for $Y\text{Co}_{12}\text{B}_6$, $Gd\text{Co}_{12}\text{B}_6$, and $Ho\text{Co}_{12}\text{B}_6$ with $\mu_0 H = 0.1$ T.

FIG. 3. Resistivity as a function of temperature for (a) $YCo_{12}B_6$, (b) $GdCo_{12}B_6$, and (c) $HoCo_{12}B_6$. Thin straight lines (red continuous lines) are linear fits to the high-temperature estimate behavior. Red circles show the estimation for electron-phonon contribution (ρ_{ph}) with a basis on the Bloch-Grüneisen theory, as explained in the text. The blue triangles are the estimation for the spin-disorder resistivity (ρ_m). The residual resistivities ρ_0 are given by the thin continuous black lines.

TABLE II. Characteristic temperatures and other parameters obtained from the resistivity and magnetization experiments on $RCo_{12}B_6$ (R = Y, Gd, and Ho).

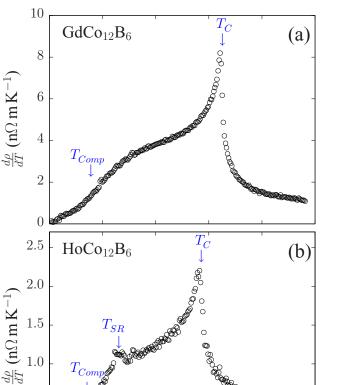| Parameters	$RCo_{12}B_6$		
	Y	Gd	Ho
T_C (K)[a]	150 ± 1	162 ± 1	145 ± 1
T_{SR} (K)[a]			76 ± 2
T_{comp} (K)[a]		49 ± 1	44 ± 1
T_C (K)[b]	148 ± 1	160 ± 1	144 ± 2
θ_R (K)[c]	125 ± 11	193 ± 9	199 ± 10
ρ_θ (nΩ m)[c]	55 ± 1	47 ± 2	28 ± 2
ρ_0 (nΩ m)	4.6 ± 0.5	2.2 ± 0.5	1.4 ± 0.5
RRR[d]	28 ± 0.5	33 ± 0.5	32 ± 0.5

[a]Obtained from M versus T.
[b]Obtained from $d\rho/dT$.
[c]Obtained from ρ_{ph} analysis.
[d]Residual-resistance ratio.

range between 150 and 300 K for the $YCo_{12}B_6$ and $GdCo_{12}B_6$ systems. The fact that a large ρ_m term is present in the Y-based compound means that the Co moments are effective to produce significant spin-disorder resistivity. On the other hand, for $HoCo_{12}B_6$ the electron-phonon term is dominant across the entire investigated temperature interval in spite of having approximately the same amplitude as in $GdCo_{12}B_6$. The saturated (above T_C) spin-disorder resistivity related to rare-earth moments, in the absence of crystal-field effects, varies as $\rho_m \propto (g_J - 1)^2 J(J + 1)$, where $(g_J - 1)^2$ is the de Gennes factor [24]. With a basis solely on the values for g_J and J for Gd and Ho, we calculate the ratio $\frac{\rho_m(Gd)}{\rho_m(Ho)} = 3.5$, which is in reasonable agreement with the ratio $\frac{\rho_m(Gd)}{\rho_m(Ho)} \approx 4$ observed at room temperature, where the spin-disorder resistivity is saturated in both systems. This finding strongly suggests that the electron scattering by the rare-earth sublattice is of fundamental importance to explain the magnetic contribution to the resistivity of the $RCo_{12}B_6$ compounds. As also seen in Fig. 3, the experimentally estimated spin-disorder resistivity of the Ho-based compound decreases a little when the temperature is increased above its maximum value at $T \approx T_C$. This small variation of the saturated spin-disorder resistivity is probably due to crystal-field effects [24].

Results for the temperature derivative of the resistivity $d\rho/dT$ are presented in Figs. 4(a) and 4(b) for $GdCo_{12}B_6$ and $HoCo_{12}B_6$, respectively. A pronounced peak in $d\rho/dT$ is observed close to the critical magnetic temperature for both systems. This behavior is related to critical magnetic fluctuations (short-range correlations) that attain the maximum intensity in a temperature slightly below the magnetic ordering temperature [25]. We adopt the peak temperature in $d\rho/dT$ to identify T_C in our samples. The so-determined critical temperatures are listed in Table II and are in very good agreement with values obtained from magnetic measurements. Anomalies are not observed in the resistivity and $d\rho/dT$ at the compensation temperature. This is expected since no particular change in the electron scattering processes occurs at T_{comp}. However, a significant anomaly is noticeable in the vicinity of T_{SR} for $HoCo_{12}B_6$, showing that the temperature dependence of the

ordering temperature, the resistivity contribution due to thermal spin disorder, which is saturated well above T_C, drops markedly upon decreasing the temperature. We estimate the spin-disorder contribution to the resistivity of the studied compounds by subtracting the calculated ρ_{ph} from the ideal resistivity $\rho_i(T) = \rho(T) - \rho_0$. The magnetic term $\rho_m(T) = \rho_i - \rho_{ph}$ is plotted as blue triangles in Fig. 3. It is interesting to observe in panels (a) and (b) of Fig. 3 that $\rho_m(T)$ is responsible for the largest resistivity contribution in the temperature

FIG. 4. Temperature derivative of the resistivity as a function of temperature for (a) $GdCo_{12}B_6$ and (b) $HoCo_{12}B_6$. Characteristic temperatures are signaled as explained in the text.

resistivity is sensitive to the spin-reorientation phenomenon in the magnetic structure of the Ho-based system.

The characteristic temperatures obtained from the magnetic and transport measurements are listed in Table II and are in very good agreement with the values found in the literature [7–16].

C. Magnetoresistance

Figure 5 displays the magnetoresistance (MR) in the perpendicular ($H \perp i$) and parallel ($H \parallel i$) configurations at $T = 2$ K for $YCo_{12}B_6$. A negative MR contribution caused by suppression of residual magnetic disorder related to domain orientation effects is observed at low fields. A partial field-induced alignment in the canted configuration of the Co moments [13,18] may also contribute to reduce the magnetic scattering rate. When the applied induction surpasses a few tenths of a tesla, a strong positive MR contribution becomes dominant. This term shows a small anisotropy with respect to the relative field-current orientation and increases quasi-linearly with the field, with a small negative curvature at the highest applied fields. The overall behavior of the MR shown in Fig. 5 is rather unusual in magnetic materials. The Lorentz force mechanism [26] may hardly explain the positive MR
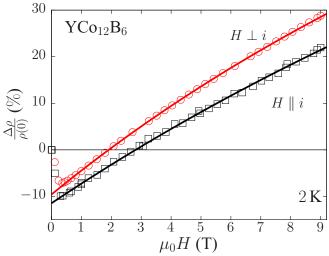

FIG. 5. Perpendicular ($H \perp i$) and parallel ($H \parallel i$) magnetoresistance as a function of the field for $YCo_{12}B_6$. Results were obtained at $T = 2$ K and are normalized by the resistivity at zero field. Continuous lines correspond to fits of Eq. (7) to the magnetoresistance data.

contribution in this case, since it predicts a rather anisotropic effect (much larger for the perpendicular configuration) that is proportional to H^2.

We propose that the positive MR at low temperatures in $YCo_{12}B_6$ is due to spin-polarized electron transport. According to the model of Campbell and Fert [27], the resistivity of a ferromagnetic metallic system is given by

$$\rho = \frac{\rho_\uparrow \rho_\downarrow + \rho_{\uparrow\downarrow}(\rho_\uparrow + \rho_\downarrow)}{\rho_\uparrow + \rho_\downarrow + 4\rho_{\uparrow\downarrow}}, \qquad (2)$$

where ρ_σ ($\sigma = \uparrow, \downarrow$) are the spin-dependent resistivities for the two spin-polarized subbands and $\rho_{\uparrow\downarrow}$ is the spin-mixing term. The spin-mixing term is a pseudoresistivity that transfers momentum from one current to the other so that an equalization of the subband resistivities occurs when the spin-polarized currents are totally mixed in the limit $\rho_{\uparrow\downarrow} \gg \rho_\sigma$ [27]. The spin-mixing term was shown to play an important role in the description of the deviations of Matthiessen's rule in dilute ferromagnetic alloys [28]. In the Campbell-Fert model, the spin-mixing is attributed to electron-magnon or spin-orbit scattering. In the present approach we suppose that, in the presence of an applied magnetic field, $\rho_{\uparrow\downarrow}$ originates mostly from the spin-flipping events induced by the Zeeman interaction.

At this point, it is important to mention that other models have been proposed to explain positive magnetoresistance in ferromagnetic systems. One of these models, proposed by Onose *et al.* [29], explains the positive magnetoresistance in $Fe_{1-x}C_xSi$ by assuming that the Zeeman splitting induces a decrease in the density of states of a minority-spin band having high mobility. In a more general context, it has been shown that band splitting at the Fermi level that originated from the spin-orbit interaction strongly influences the anisotropic magnetotransport properties of ferromagnetic metals and compounds [27,30–33] by affecting the scattering of s-type conduction electrons into localized d-states.

TABLE III. Parameters derived from fitting Eq. (7) to magnetoresistance measurements in Figs. 5 and 7.

Parameters	Y (MRL)	Y (MRT)	Gd (MRL)	Gd (MRT)
C	2.20	1.95	0.99	22.72
H_0	51.15	36.95	9.87	162.54
$D (\times 10^{-2})$	−11.46	−9.59	−3.84	−1.67

Considering that $\rho_{\uparrow\downarrow}$ is negligible at zero applied field and low temperatures [27,28], and assuming that the subband resistivities remain unaltered in the studied field range, the MR may be written as

$$\Delta\rho(H) = \frac{(\rho_\uparrow + \rho_\downarrow)^2 - 4\rho_\uparrow\rho_\downarrow}{(\rho_\uparrow + \rho_\downarrow)[\rho_\uparrow + \rho_\downarrow + 4\rho_{\uparrow\downarrow}(H)]} \rho_{\uparrow\downarrow}(H), \quad (3)$$

where $\Delta\rho(H) = \rho(H) - \rho(0)$ and $\rho(0) = \rho_\uparrow\rho_\downarrow/(\rho_\uparrow + \rho_\downarrow)$.

Equation (3) has two simple limits. When $\rho_{\uparrow\downarrow} \ll \rho_\sigma$, one obtains

$$\Delta\rho(H) \simeq \left(\frac{\mu - 1}{\mu + 1}\right)^2 \rho_{\uparrow\downarrow}(H), \quad (4)$$

where $\mu = \rho_\downarrow/\rho_\uparrow$ is the spin-polarization ratio [28]. In the limit $\rho_{\uparrow\downarrow} \gg \rho_\sigma$, the MR is saturated and given by

$$\Delta\rho(\infty) = \frac{(\mu - 1)^2}{4\mu}\rho(0). \quad (5)$$

Equation (5) shows that the mixing of spin-polarized currents may produce positive and large magnetoresistance when compared to the zero-field resistivity, depending on the value of the spin-polarization ratio. Considering that $\rho_{\uparrow\downarrow}$ originates mostly from the Zeeman coupling, we suppose that

$$\rho_{\uparrow\downarrow}(H) = a_Z H, \quad (6)$$

where the phenomenological constant a_Z may depend on the temperature. Within this approximation, Eq. (4) predicts that the MR increases linearly with H at very low fields, much as is observed in Fig. 5. Substituting relation (6) in Eq. (3), we write the magnetoresistance as

$$\frac{\Delta\rho(H)}{\rho(0)} = C \frac{H}{H_0 + H} + D. \quad (7)$$

The parameters in Eq. (7) are $C = (\mu - 1)^2/4\mu$ and $H_0 = (\mu + 1)^2\rho(0)/4a_Z\mu$. The constant D takes approximately into account the negative contribution to $\Delta\rho$ related to any field-induced process that favors magnetic ordering. Fitting Eq. (7) to results in Fig. 5 allows an estimation of the spin-polarization ratio and the phenomenological constant a_Z. In Table III, we collect the parameters derived from these fits to the MR results in the studied systems. For instance, for $YCo_{12}B_6$ in the geometry $H \parallel i$, we obtain $\mu_\parallel = 0.09$ and $a_Z(\parallel) = 2.9$ nΩ m/T. The reciprocal $\mu_\parallel^{-1} = 10.7$ is also a possible solution. We assume that $\mu < 1$ with a basis on the observed MR anisotropy, with $\Delta\rho(\perp)$ being larger than $\Delta\rho(\parallel)$. Results for the spontaneous resistivity anisotropy (see the Supplemental Material [34]) are in accordance with our assumption. According to our interpretation, the minority-spin subband dominates the resistivity in $YCo_{12}B_6$. Nonpolarized band calculations in $YCo_{12}B_6$ show that the Fermi energy is
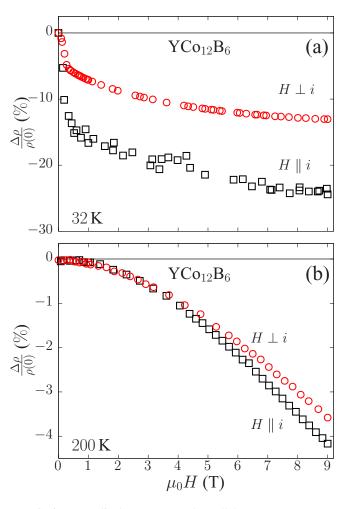

FIG. 6. Perpendicular ($H \perp i$) and parallel ($H \parallel i$) magnetoresistance as a function of the field for $YCo_{12}B_6$. Results obtained at $T = 32$ and 200 K are shown in panels (a) and (b), respectively.

located in a region with a peaked density of states [35]. This result suggests that spin-polarized currents with rather distinct intensities flow when the internal exchange field of the Co sublattice is taken into account.

The anisotropy of the magnetoresistance (AMR) with respect to the current-field relative orientation observed in Fig. 5 is often attributed to single-ion scattering depending on the spin-orbit interaction and crystal-field effects [27]. The coupling of the applied field with the canted and incommensurate magnetic structure of the Co sublattice [13,17,18] may also play a role in explaining AMR in the studied compounds. This effect is taken into account by the constant D in Eq. (7). From the fit of Eq. (7) to data for $H \perp i$ in Fig. 5 we obtain $\mu_\perp = 0.10$ and $a_Z(\perp) = 3.7$ nΩ m / T. The fitting procedure indicates that the ratio μ remains largely insensible to the current-field configuration, whereas H_0 has different values. This result suggests that an additional contribution to the anisotropy in the results of Fig. 5 comes from the coupling constant a_Z. In other words, a significant contribution to AMR in $YCo_{12}B_6$ is due to the spin-mixing resistivity $\rho_{\uparrow\downarrow}(H)$.

The strong and positive magnetoresistance seen at 2 K in $YCo_{12}B_6$ due to the spin-mixing effect decreases strongly with increasing temperatures. As shown in Fig. 6(a), at $T =$
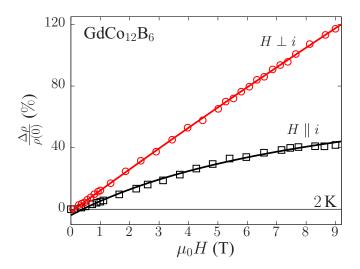
FIG. 7. The same as Fig. 5, but for GdCo$_{12}$B$_6$.

FIG. 8. The same as Fig. 6, but for GdCo$_{12}$B$_6$. Panels (a) and (b) shows MR results obtained at $T = 60$ and 200 K, respectively.

32 K the MR is dominated by the suppression of spin disorder. At this temperature, the anisotropy originating from the spin-orbit interaction is particularly pronounced. In panel (b) of the same figure, MR results above T_C are shown. The usual and small MR characteristic of the paramagnetic state is observed in this case, where a residual anisotropy due to spin-orbit coupling is still visible (additional MR measurements for YCo$_{12}$B$_6$ are shown in the Supplemental Material [34]).

Figure 7 shows the normalized magnetoresistance of the GdCo$_{12}$B$_6$ compound at $T = 2$ K. Measurements were carried out for both ($H \perp i$) and ($H \parallel i$) configurations. These results are quite surprising. The large amplitude of $\Delta\rho/\rho(0)$, which attains over 100% at $\mu_0H = 9$ T in the ($H \perp i$) geometry, as well as the large anisotropy with respect to the current-field relative orientations, are unusual features that hardly can be understood from the standpoint of the ordinary Lorentz-force contribution. Equation (7), however, could be quite well fitted with reasonable parameters to MR results in Fig. 7. The D constants for both geometries are quite small for the Gd-based system, showing that residual spin disorder is almost negligible in this compound. For the ($H \parallel i$) configuration, we estimate $\mu_\parallel = 0.17$ and $a_Z(\parallel) = 4.5$ nΩ m/T, which are values similar to those encountered in YCo$_{12}$B$_6$. For ($H \perp i$), the magnetoresistance is quasilinear with the field, with an almost imperceptible negative curvature. Then the adjustable parameters in the fitting procedure using Eq. (7) are prone to large uncertainties. Nevertheless, we derive $\mu_\perp = 0.01$ and $a_Z(\perp) = 3.2$ nΩ m/T. As for YCo$_{12}$B$_6$, the coupling constant a_Z is moderately anisotropic in GdCo$_{12}$B$_6$. On the other hand, the polarization rate is extremely small for the ($H \perp i$) geometry. This means that, for this current-field configuration, GdCo$_{12}$B$_6$ behaves almost as a half-metal where only minority electrons are present near the Fermi level.

An extension of the Campbell-Fert spin-mixing model proposed by Kokado *et al.* [33] might take into account anisotropic spin-polarization ratios. However, it seems improbable that the spin-orbit interaction is solely responsible for the extremely large anisotropy estimated for μ in GdCo$_{12}$B$_6$. We suggest that the antiferromagnetic coupling between the Gd and Co moments [15] may play a crucial
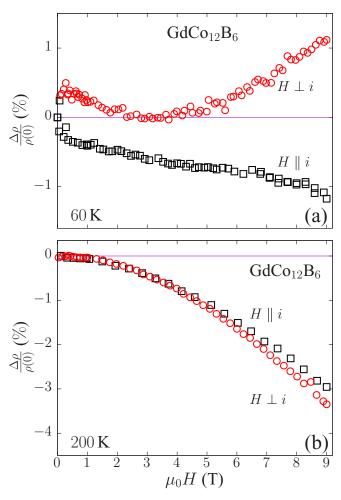
role by opening a narrow pseudogap in the energy spectrum near the Fermi level. Coupled to the spin-orbit interaction, this pseudogap would produce a severe depletion in the density of majority electrons, leading to an enormous increase in $\rho(\uparrow)$ and, consequently, to an extremely small value for the spin-polarization ratio in the ($H \perp i$) configuration.

The positive magnetoresistance due to the spin-mixing mechanism subsists up to temperatures a little above T_{comp} in GdCo$_{12}$B$_6$. Figure 8 shows representative MR results for this system at $T = 60$ and 200 K. It is interesting to observe that the MR results above T_C are quite similar for both YCo$_{12}$B$_6$ and GdCo$_{12}$B$_6$ compounds [see Figs. 6(b) and 8(b)]. This means that at high temperatures, the electrical transport properties of these systems are dominated by the Co sublattice.

Further MR measurements in the Gd-based system are presented in the Supplemental Material [34]. Magnetoresistance results for HoCo$_{12}$B$_6$ in the ($H \perp i$) configuration are also shown in the Supplemental Material [34]. Experiments could not be performed in the parallel geometry for this system. Available results are quantitatively and qualitatively similar to corresponding experiments in GdCo$_{12}$B$_6$. This is expected since the magnetic ordered states in the Gd-based and Ho-based compounds are analogous, with similar critical and
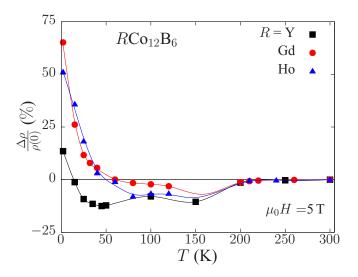
FIG. 9. Amplitude of the perpendicular magnetoresistance measured at $\mu_0 H = 5$ T as a function of the temperature for the $RCo_{12}B_6$ ($R =$ Y, Gd, and Ho) compounds.

compensation temperatures, the rare-earth moments pointing antiparallel to the Co magnetization in both cases.

In Fig. 9, we plot the MR amplitude measured in the ($H \perp i$) geometry at $\mu_0 H = 5$ T as a function of the temperature for the three studied systems. This figure emphasizes the similarities of the results for the different systems. At low temperatures, the MR is strong and positive, dominated by the spin-mixing mechanism. At temperatures near T_{comp} the MR changes sign and suppression of spin disorder becomes prominent. Near the critical temperature, the MR due to spin disorder goes through a maximum that may be associated with enhanced scattering by spin chiralities, as observed in the Hall resistivity results discussed in the next section.

D. Hall resistivity

Representative measurements of isotherm Hall resistivity ρ_{xy} as functions of the applied magnetic field for the $GdCo_{12}B_6$ compound are shown in Fig. 10. Qualitatively similar results were obtained for the Y-based and Ho-based systems (see the Supplemental Material [34]). The results depicted in Fig. 10 are typical of magnetic materials where the Hall resistivity is usually written as [36,37]

$$\rho_{xy} = R_0 B + R_S \mu_0 M. \tag{8}$$

In the phenomenological Eq. (8), the first term is the ordinary contribution to the Hall resistivity, where B is the magnetic induction. The second term is known as the anomalous Hall effect (AHE), which is proportional to the material's magnetization M. The parameters R_0 and R_S are the ordinary and anomalous Hall coefficients, respectively. The constant μ_0 is the vacuum permeability.

Also useful is the representation of the Hall effect data in terms of the total Hall coefficient R_H defined as
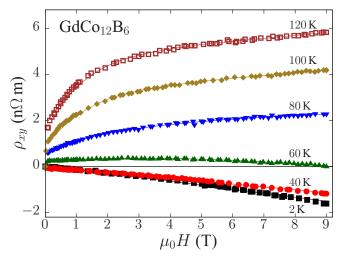
$$R_H = \rho_{xy}/\mu_0 H. \tag{9}$$

FIG. 10. Hall resistivity as a function of the applied field for $GdCo_{12}B_6$ in some fixed temperatures.

Figure 11 shows the total Hall coefficient for the three studied systems as a function of the reduced temperature T/T_C in the fixed applied field $\mu_0 H = 5$ T. In this figure, the R_H data for each compound are normalized with respect to the value at T_C in order to emphasize their qualitative similitude in the different compounds.

Results like those shown in Figs. 10 and 11 may be understood from the standpoint of Eq. (8) and the two-band model for the Hall effect [26]. In the case of the studied systems, the spin-polarized subbands play the role of the two different electron bands. Moreover, in accordance with the interpretation given to the magnetoresistance results, we consider that at the Fermi level the highly resistive majority band is almost full and holelike, whereas the low-resistive minority band is electronlike. Then, we write the expression
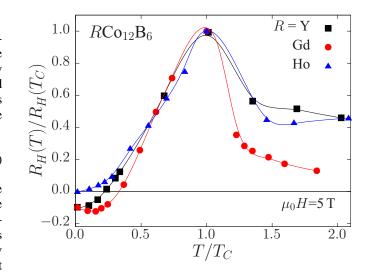

FIG. 11. Total Hall coefficient measurements at $\mu_0 H = 5$ T for $RCo_{12}B_6$ ($R =$ Y, Gd, and Ho) plotted as functions of T/T_C. Data are normalized to the value at T_C. Values for $R_H(T_C)$ are 0.65×10^{-9}, 1.5×10^{-9}, and 0.42×10^{-9} m^3/C for Y-, Gd-, and Ho-based compounds, respectively.

for the Hall coefficient in the two-band model as

$$R_H = \frac{\mu^2 R_h(\uparrow) - R_e(\downarrow)}{(\mu + 1)^2}. \tag{10}$$

In the above expression, $R_{h(e)}(\sigma)$ are the Hall coefficients for the hole (electron) spin-polarized subbands. Both coefficients are assumed to be positive quantities. At low temperatures and low applied fields, the spin-mixing term $\rho_{\uparrow\downarrow}$ may be supposed negligible. Then Eq. (10) is valid and R_H is expected to be negative since $\mu \ll 1$ in our compounds. This behavior is indeed observed in the results shown in Figs. 10 and 11. When temperature increases, currents become mixed. In the limit of complete mixing, both subbands have resistivity $\frac{1}{2}(\rho_\uparrow + \rho_\downarrow)$, so that $\mu = 1$. Consequently, in the high-temperature limit, the Hall constant becomes $R_H = \frac{1}{4}[R_h(\uparrow) - R_e(\downarrow)]$ and may be positive, as experimentally observed.

Comparing results in Figs. 9 and 11, one remarks that the temperature where R_H changes sign is practically coincident with that where sign reversal of the MR occurs for each studied compound. This indicates that the origin of the sign reversal in both the MR and Hall effect is the spin-mixing phenomenon, which has to be properly considered in any system where spin-polarized electrical transport is relevant. In the low-temperature results of Fig. 10, the negative Hall resistivity varies almost linearly with the field and is basically due to the ordinary Hall effect. At $T \approx 60$ K, the sign reversal occurs and the anomalous contribution becomes dominant, since ρ_{xy} at fixed temperatures mimics the behavior of the magnetization as a function of the applied field. The magnitude of ρ_{xy} goes through a maximum at temperatures near T_C, then decreases upon increasing the temperature. The linear dependence with the field is restored, though with positive slope.

Using Eq. (8), expression (9) may be rewritten as

$$R_H = R_0 + \chi_M R_S. \tag{11}$$

In the above expression, the quantity $\chi_M = M/(H + M)$ takes into account that the demagnetizing factor is maximum for the Hall geometry [38]. In high values of the applied field, for which the technical saturation magnetization is achieved, Eq. (11) shows that R_H is a linear function of χ_M for a fixed temperature. Then, plots of the experimentally measured R_H versus χ_M allows the determination of $R_0(T)$ and $R_S(T)$ in the limit of high applied fields. In the Supplemental Material [34], representative examples of these plots are shown for the studied systems. Analysis of the R_H data with Eq. (11) shows that the ordinary contribution is negative and dominant in the low-temperature range ($T < 50$ K) in all systems. In high temperatures ($T > 200$ K), R_0 becomes positive. In the regime 50 K $< T < T_C$ the anomalous contribution is largely dominant, with positive R_S in all studied compounds. In this temperature interval, R_0 is small and changes sign. However, its determination is prone to large uncertainties.

We focus on the anomalous coefficient for a quantitative analysis of the data in Fig. 11 with Eq. (11). In Fig. 12, we show the values obtained for R_S in the three investigated compounds as a function of the temperature at the fixed field $\mu_0 H = 5$ T. These results do not depend significantly on the
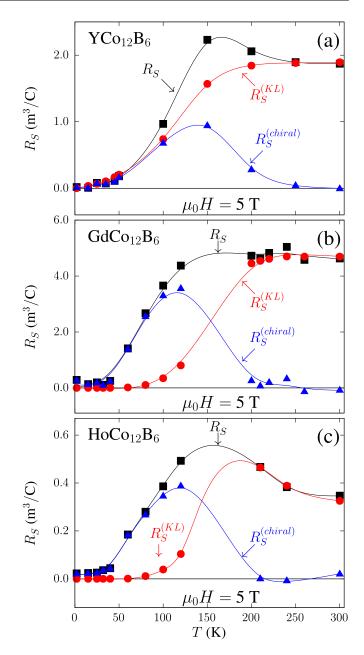

FIG. 12. Anomalous Hall coefficient as a function of the temperature deduced from analyses based on Eq. (11) with the field $\mu_0 H = 5$ T. Data for $RCo_{12}B_6$, where $R = $ Y, Gd, and Ho are shown as black squares in panels (a), (b), and (c), respectively. Estimate for the KL (red circles) and chiral (blue triangles) contributions for R_S are also presented (see text).

applied field in the range $3 < \mu_0 H < 9$ T. One immediately observes that the curve $R_S(T)$ for each sample is reminiscent of the respective magnetic resistivity $\rho_m(T)$ shown in Fig. 3, mostly in the low- and high-temperature ranges. This resemblance is not surprising since theoretically R_S is expected to scale with the longitudinal resistivity [37]. According to the skew scattering mechanism for the AHE, $R_S \propto \rho_m$, whereas the intrinsic Karplus-Luttinger (KL) contribution predicts that $R_S \propto \rho_m^2$ [37]. The skew scattering, i.e., the asymmetric scattering produced by the spin-orbit interaction, is usually

associated with the presence of impurities or disorder [39]. The KL term is understood in terms of the Berry phase and Berry curvature of band states in the k-space [40]. This contribution leads to an anomalous contribution to the Hall conductivity, which is largely independent of scattering. Then, the inversion of the conductivity tensor leads to an anomalous Hall resistivity, which varies as the square of the longitudinal resistivity [37]. It is likely that both the skew scattering and the KL terms should be taken into account to precisely describe our anomalous Hall data. Our results, however, do not suggest which of these contributions is the most important. We then adopt a practical rule based on the review of Nagaosa *et al.* [37]. According to these authors, in good metals where $10^{-6} < \rho < 10^{-4}$ Ω cm, the intrinsic KL contribution is dominant. Skew scattering is mostly prominent in high conductivity materials ($\rho < 10^{-6}$ Ω cm). To estimate the KL term, we assume that $R_S = a\rho_m^2$ in the high-temperature limit, where both quantities are clearly proportional to each other. Using the proportionality constant a so derived and the ρ_m data of Fig. 3, we plot the curves labeled as $R_S^{(KL)}$ in Fig. 12.

Despite the fact that the measured R_S in the high- and low-temperature limits are described well, large deviations between experiments and $R_S^{(KL)}$ are observed in the intermediate temperature range, which encompasses T_C. We then calculate and plot in Fig. 12 the quantity $R_S^{(chiral)} = R_S - R_S^{(KL)}$. This quantity goes through a maximum at $T \approx T_C$ for YCo$_{12}$B$_6$ and $T \lesssim T_C$ for GdCo$_{12}$B$_6$ and HoCo$_{12}$B$_6$, then fades away in the low- and high-temperature ranges for all systems. Based on this general behavior, we interpret $R_S^{(chiral)}$ as a contribution of spin chiralities to the anomalous Hall effect, as much as theoretically proposed by Kawamura and Tatara in the context of metallic spin glasses [41,42]. Spin chiralities defined as $\chi_{ch} = \mathbf{S}_i \cdot \mathbf{S}_j \times \mathbf{S}_k$ are relevant to non-coplanar spin structures. Successive elastic scattering by the three local spins in χ_{ch} generates a fictitious magnetic field, leading to an additional contribution to the Hall current when a uniform chirality is achieved under the application of an external magnetic field [43]. The chiral term is a real-space analog of the Berry phase mechanism generating the KL contribution, although its occurrence depends on the additional requirement of spin canting. Experimental studies of the chiral contribution to the Hall effect have been made in oxide ferromagnets, as the manganites [37]. Measurements in these systems led to a pioneering theoretical proposal for the existence of a real-space Berry phase anomalous Hall effect in the case of hopping-type transport [44]. Experiments pointing out a chiral contribution to AHE were also carried out in metallic systems such as the spin glass and reentrant AuFe alloys [45]. More recently, a Hall resistivity of chiral origin has been reported to occur in the skyrmion phase of complex magnetic materials [46]. The chiral term is expected to be strongly affected by the local spin dynamics. The maximum of this contribution occurring near the Curie temperature is an indication that the typical time involved in the coherent scattering of conduction electrons by chiralities remains shorter than the corresponding time for spin precession in this temperature range. At low temperatures, the chiral term decreases strongly in our compounds probably because of their good crystalline and spin ordering. This finding is consistent with the small

magnetic contribution to their longitudinal resistivity in the same temperature region.

IV. SUMMARY

A systematic investigation of the temperature dependence of the electronic transport properties of YCo$_{12}$B$_6$, GdCo$_{12}$B$_6$, and HoCo$_{12}$B$_6$ was carried out. The study includes resistivity, magnetoresistance, and Hall effect measurements performed in the temperature range 2–300 K, in the presence of applied fields up to 9 T.

The residual resistivity of the studied materials was found to be remarkably small, due to the complexities of their crystal structure and magnetic phase diagram. The temperature-dependent resistivity behaves as in standard ferromagnetic materials and could be described with a basis on two main contributions. One of them is due to the electron-phonon interaction and the other term has a magnetic origin, being related to electron scattering by spin excitations. Above the Curie temperature, the magnetic term is essentially constant, as expected within the simple spin-disorder scenario. No signature of the compensation temperature is seen in the ρ versus T curves for the Gd- and Ho-based compounds. However, a clear anomaly is observed in $d\rho/dT$ at the spin-reorientation temperature in the case of HoCo$_{12}$B$_6$.

The magnetoresistance of all studied compounds presents a quite unusual behavior at low temperatures. It is positive, presents a negative curvature with increasing field, and has a rather large amplitude when compared to that characterizing most metallic and magnetic systems. The magnetoresistance for YCo$_{12}$B$_6$ is almost isotropic with respect to the relative orientation of current and field, while in GdCo$_{12}$B$_6$ the MR is much larger when $H \perp i$. For interpreting the results in the limit of low temperatures, we proposed a scenario based on the two-current model devised by Campbell and Fert [27]. According to this theory, two spin-polarized subbands carry the current in parallel, and spin mixing is taken into account via a pseudoresistivity term. According to our interpretation, the MR is basically due to the spin-mixing resistivity, and its amplitude is crucially dependent on the spin-polarization ratio. Fits of the expression derived from the model to the experimental MR results for YCo$_{12}$B$_6$ and GdCo$_{12}$B$_6$ allow us to estimate the spin-polarization ratio for these two compounds. We find that $\rho(\uparrow)/\rho(\downarrow) < 1$ in both compounds. Although the two-current model may account for the moderate MR anisotropy observed in YCo$_{12}$B$_6$, a mechanism specifically dependent on the magnetic rare earths appears to be important to explain the much larger effect occurring in the Gd-based compound.

The Hall effect experiments in the three studied compounds clearly show the occurrence of an anomalous term proportional to the magnetization in addition to the ordinary effect due to the Lorentz curvature of the electron trajectories. In all compounds, the total Hall coefficient is negative at low temperatures, but shows a sign reversal upon increasing T up to 60 K, approximately. The analysis of these results led us to conclude that the highly resistive majority-spin subband is holelike whereas the low-resistivity minority-spin subband is electronlike. Using auxiliary magnetization data, we were able

to separate the anomalous Hall resistivity from the ordinary one. According to our analysis, two contributions are relevant to explain the AHE in the studied systems. One of them is the intrinsic Karplus-Luttinger term while the other is a chiral term that attains its maximum amplitude in temperatures near T_C.

As an overall conclusion, our experimental work on the resistivity and magnetotransport properties of $R\mathrm{Co}_{12}\mathrm{B}_6$ ($R =$ Y, Gd, and Ho) revealed that the electrical conduction in these materials is basically a property of spin-polarized bands related to the cobalt sublattice. In this sense, our measurements are in accordance with previous studies on the magnetic properties of these systems that attribute an itinerant character to the magnetism of the Co sublattice. Our detailed magnetoresistance and Hall effect results, suggesting that minority- (majority-) spin subbands have hole (electron) character, are a guide for yet-to-come electronic band calculations

in the ordered phase of the $R\mathrm{Co}_{12}\mathrm{B}_6$ compounds. However, a complete description of the anomalous Hall effect needs to consider that the Co spins manifest canting, and consequently they also show a local character to some extent. This point might deserve further investigations on the detailed magnetic structure of these systems, preferably based on neutron diffraction experiments.

[1] C. Kaiser, A. F. Panchula, and S. S. P. Parkin, Phys. Rev. Lett. **95**, 047202 (2005).

[2] A. Kirilyuk, A. V. Kimel, and T. Rasing, Rev. Mod. Phys. **82**, 2731 (2010).

[3] J. Hohlfeld, T. Gerrits, M. Bilderbeek, T. Rasing, H. Awano, and N. Ohta, Phys. Rev. B **65**, 012413 (2001).

[4] S. P. Lee, C. K. Kim, K. Nahm, M. Mittag, Y. H. Jeong, and C.-M. Ryu, J. Appl. Phys. **81**, 2454 (1997).

[5] M. Misek, Z. Arnold, O. Isnard, H. Mayot, Y. Skorokhodaan, and J. Kamarad, Acta Phys. Pol. A **113**, 263 (2008).

[6] F. Mesquita, L. V. B. Diop, G. Fraga, O. Isnard, and P. Pureur, IEEE Mag. Lett. **6**, 1 (2015).

[7] K. Niihara and S. Yajima, Chem. Lett. **1**, 875 (1972).

[8] M. Mittag, M. Rosenbreg and K. Buschow, J. Magn. Magn. Mater. **82**, 109 (1989).

[9] L. V. B. Diop and O. Isnard, Appl. Phys. Lett. **108**, 132401 (2016).

[10] L. V. B. Diop, O. Isnard, and J. Rodríguez-Carvajal, Phys. Rev. B **93**, 014440 (2016).

[11] L. V. B. Diop and O. Isnard, Phys. Rev. B **97**, 014436 (2018).

[12] L. V. B. Diop and O. Isnard, J. Alloys Compd. **688**, 953 (2016).

[13] L. V. B. Diop, O. Isnard, N. R. Lee-Hone, D. H. Ryan, and J. M. Cadogan, J. Phys.: Condens. Matter **25**, 316001 (2013).

[14] M. Rosenberg, M. Mittag, and K. H. J. Buschow, J. Appl. Phys. **63**, 3586 (1988).

[15] N. Duc, T. Hien, D. Givord, J. Franse, and F. de Boer, J. Magn. Magn. Mater. **124**, 305 (1993).

[16] O. Isnard, Y. Skourski, L. V. B. Diop, Z. Arnold, A. Andreev, J. Wosnitza, A. Iwasa, A. Kondo, A. Matsuo, and K. Kindo, J. Appl. Phys. **111**, 093916 (2012).

[17] L. V. B. Diop and O. Isnard, J. Phys.: Condens. Matter **27**, 026004 (2015).

[18] L. V. B. Diop, Z. Arnold, O. Isnard, and J. Kamarád, J. Alloys Compd. **593**, 163 (2014).

[19] M. Kawakami and S. Satohira, J. Magn. Magn. Mater. **104–107**, 1313 (1992), Proceedings of the International Conference on Magnetism, Part II.

[20] K. Erdmann, M. Rosenberg, and K. H. J. Buschow, J. Appl. Phys. **63**, 4113 (1988).

[21] J. M. Cadogan, S. J. Campbell, X. L. Zhao, H. S. Li, and P. W. Thompson, in *Hyperfine Interactions (C)*, edited by M. F. Thomas, J. M. Williams, and T. C. Gibb (Springer, Dordrecht, 2002), pp. 119–122.

[22] A. Barlet, J. Genna, and P. Lethuillier, Cryogenics **31**, 801 (1991).

[23] G. T. Meaden, *Electrical Resistance of Metals*, 1st ed. (Plenum Press, New York, 1965).

[24] V. U. S. Rao and W. E. Wallace, Phys. Rev. B **2**, 4613 (1970).

[25] P. L. Rossiter, *The Electrical Resistivity of Metals and Alloys*, 1st ed. (Cambridge University Press, Cambridge, 1987).

[26] J. Ziman, *Principles of the Theory of Solids*, 2nd ed. (Cambridge University Press, Cambridge, 1972).

[27] I. A. Campbell and A. Fert, *Transport Properties of Ferromagnets*, 1st ed. (North-Holland, Amsterdam, 1982).

[28] A. Fert and I. A. Campbell, J. Phys. F **6**, 849 (1976).

[29] Y. Onose, N. Takeshita, C. Terakura, H. Takagi, and Y. Tokura, Phys. Rev. B **72**, 224431 (2005).

[30] J. Smit, Physica **17**, 612 (1951).

[31] R. I. Potter, Phys. Rev. B **10**, 4626 (1974).

[32] W. Gil, D. Görlitz, M. Horisberger, and J. Kötzler, Phys. Rev. B **72**, 134401 (2005).

[33] S. Kokado, M. Tsunoda, K. Harigaya, and A. Sakuma, J. Phys. Soc. Jpn. **81**, 024705 (2012).

[34] See Supplemental Material at http://link.aps.org/supplemental/10.1103/PhysRevB.101.224414 for additional magnetoresistance, spontaneous anisotropy of the resistivity, and Hall resistivity measurements on $R\mathrm{Co}_{12}\mathrm{B}_6$ ($R =$ Y, Gd, and Ho).

[35] G. Miletić and Z. Blazina, J. Magn. Magn. Mater. **323**, 2340 (2011).

[36] C. Hurd, *The Hall Effect in Metals and Alloys*, 1st ed. (Plenum Press, New York, 1972).

[37] N. Nagaosa, J. Sinova, S. Onoda, A. H. MacDonald, and N. P. Ong, Rev. Mod. Phys. **82**, 1539 (2010).

[38] R. D. Barnard and I. Ul-Haq, J. Phys. F **18**, 1253 (1988).

[39] A. Fert and A. Friederich, Phys. Rev. B **13**, 397 (1976).

[40] T. Jungwirth, Q. Niu, and A. H. MacDonald, Phys. Rev. Lett. **88**, 207208 (2002).

[41] G. Tatara and H. Kawamura, J. Phys. Soc. Jpn. **71**, 2613 (2002).

[42] H. Kawamura, Phys. Rev. Lett. **90**, 047202 (2003).

[43] G. Tatara and H. Kohno, Phys. Rev. B **67**, 113316 (2003).

[44] J. Ye, Y. B. Kim, A. J. Millis, B. I. Shraiman, P. Majumdar, and Z. Tešanović, Phys. Rev. Lett. **83**, 3737 (1999).

[45] F. W. Fabris, P. Pureur, J. Schaf, V. N. Vieira, and I. A. Campbell, Phys. Rev. B **74**, 214201 (2006).

[46] R. Ritz, M. Halder, M. Wagner, C. Franz, A. Bauer, and C. Pfleiderer, Nature (London) **497**, 231 (2013).